Experimental studies of positron stopping in matter: the binary sample method

1993 J. Phys.: Condens. Matter 5 8117

(http://iopscience.iop.org/0953-8984/5/43/023)

J. Phys.: Condens. Matter 5 (1993) 8117–8128. Printed in the UK

Experimental studies of positron stopping in matter: the binary sample method

P G Coleman, J A Baker and N B Chilton
School of Physics, University of East Anglia, Norwich NR4 7TJ, UK

Received 11 June 1993

Abstract. The measurement of implantation profiles and median implantation depths for keV positrons in solids is described. Details of the experimental technique, which is based on the difference between positron annihilation lineshape parameters in two materials that otherwise appear similar to the incident positrons, are presented, using the examples of aluminium–glass and gold–tungsten. Criteria for the suitability of the two elements of the binary sample are discussed, as are limiting factors such as post-implantation diffusion and trapping at interfaces.

1. Introduction

The establishment of a fully quantitative description of positron stopping in solids is not only a necessary prerequisite for the reliable analysis of defect profile data obtained using positron implantation spectroscopy, but also provides a stringent test of formalisms used for the description of *electron* penetration, which is important in the interpretation of data from a range of spectroscopic techniques.

Owing to the difficulties in performing direct experimental measurements researchers have often, as in the case of electrons, made use of powerful computer simulations to gain valuable insights into particle implantation. In the electron methods predictions of inelastic mean free path and stopping profiles will always be heavily reliant on Monte Carlo simulations. The paths of positrons in a material, however, can in principle be traced, and conclusive experimental support for the Monte Carlo codes can thus be gained.

The need for an exact description of positron stopping is highlighted by a brief review of the analysis associated with the deconvolution of the most simple of defect distributions—the overlayer system depicted in figure 1. Here let us assume that both overlayer and substrate are defect free, but that defects can exist in the interface. After injection into the sample, at incident energy E, the positrons rapidly reach thermal equilibrium with the lattice with a characteristic implantation profile $P(E, z)$ from which they will diffuse to be annihilated from either bulk or overlayer unlocalized states or, if encountering the surface or interface, will be trapped and annihilated there.

The fractions F_S and F_i of positrons trapped and annihilated at the surface or interface, respectively, are given by

$$F_S(E) = \int_0^\infty P(E, z) \exp(-z/L)\, dz \tag{1}$$

and

$$F_i(E) = \int_0^d P(E, z) \exp\left(\frac{z-d}{L_A}\right) dz + \int_d^\infty P(E, z) \exp\left[-\left(\frac{z-d}{L_B}\right)\right] dz \tag{2}$$

0953-8984/93/438117+12$07.50

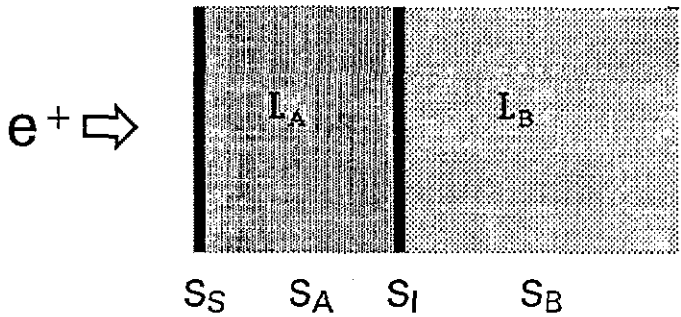

Figure 1. A schematic representation of a simple binary sample AB: L_A and L_B are the positron diffusion lengths in A and B: S_A and S_B are the S-parameters for A and B, and S_S and S_I the S-parameters associated with annihilations at the surface of the sample and at the AB interface.

where L, L_A and L_B are the positron diffusion lengths of the respective solids. Clearly in this situation the calculated fractions are strongly influenced by the magnitude of $P(E, z)$ in the vicinity of $z = 0$ and $z = d$. (Analysis is further complicated if $P(E, z)$ and the positron backscattering coefficients are substantially different in A and B.) When considering applications to extended, smoothly varying, defect distributions, as discussed by Schultz and Lynn [1], this problem is somewhat reduced. However, the calculations of the number of positrons backdiffusing to the surface will always reflect the exact functional form of $P(E, z)$ in the surface region.

Figure 2 shows $P(E, z)$ for 5 keV positrons in Al and illustrates the variety of profiles measured or simulated before those reported in this paper. Recent studies [2] of positron implantation in multilayered structures have been successfully modelled using the Gaussian derivative form ($m = 2$) of the Makhovian implantation profile

$$P(E, z) = (mz^{m-1}/z_0^m) \exp[-(z/z_0)^m]. \tag{3}$$

Modelling multilayer data is, however, relatively insensitive to profile shape, and therefore does not offer conclusive support for this functional form for $P(E, z)$. Measurements of backdiffusion in Si [3], and the only direct determination of $P(E, z)$, by measuring the positron flux transmitted through a wedge shaped sample [4], both yielded $P(E, z)$ that were non-Makhovian in form. The Monte Carlo simulations of Valkealahti and Nieminen [5] were found to be well approximated by equation (3); those of Ghosh *et al* [6] are fitted well by a functional form different from, but similar to, a Makhovian.

The value of $\bar{z}$ (or $z_{1/2}$) associated with the profile $P(E, z)$ employed is more important to the reliable modelling of results from depth profiling experiments using positron implantation spectroscopy than is the adoption of an accurate functional form for the profile. This is illustrated by the substantial differences between $\bar{z}$ values for the Monte Carlo simulations in figure 2, which would be the *prime* cause of difference between the conclusions drawn about a given experimental system modelled using the different profiles shown in the figure. Care is nevertheless required when making comparisons based on $\bar{z}$ and $z_{1/2}$ values, as confusion between the two has in the past led to misrepresentation of results.

Traditionally it has been the mean implantation depth $\bar{z}$ that has been used more widely to characterize $P(E, z)$. This is somewhat unfortunate because the parameter extracted with the most ease from experiment is the median penetration depth $z_{1/2}$. Mills and Wilson [4]

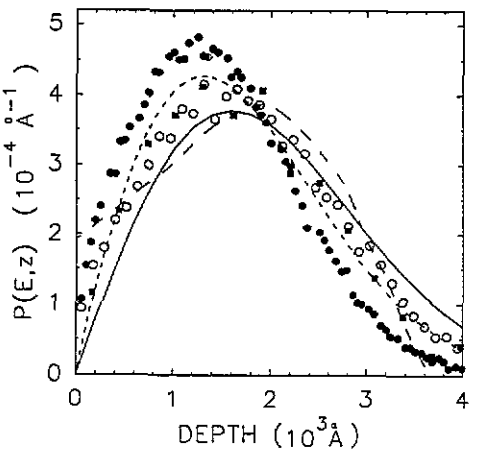

Figure 2. Implantation profiles for 5 keV positrons in Al. The filled circles show the Monte Carlo simulation results of Ghosh *et al* [6]. Other Monte Carlo results include the original simulations of Valkealahti and Nieminen [5] (filled squares), which were fitted to a Makhovian with $m = 1.9$ (short-dashed curve), and the more recent work of Jensen and Walker [11] (open circles). The only direct experimental measurements are due to Mills and Wilson [4] (long-dashed curve). The full curve is representative of the *widely advocated Gaussian derivative profile used to* fit glass multilayer results by Vehanen *et al* [2]. All profiles have been normalized so that the area under the respective curve is unity. The reader should note that in many studies the profiles are normalized such that the *total* number of incident particles (stopped *and backscattered*) corresponds to unity.

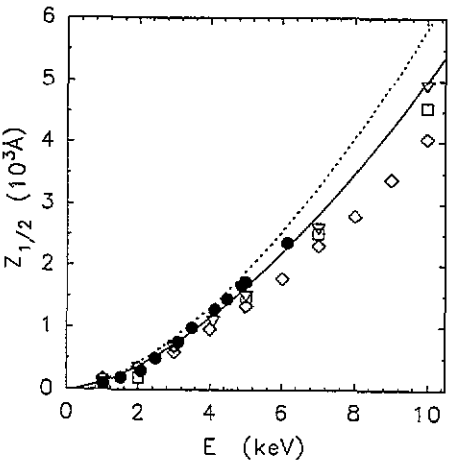

Figure 3. Median penetration depths for 0–12 keV positrons in Al. The filled circles are the experimental measurements of Mills and Wilson [4] and the full curve their fit $(332/\rho)E^{1.6}$. The broken curve is the empirical law favoured by Vehanen *et al* [2], i.e. $(377/\rho)E^{1.62}$. The fit most often quoted in positron literature (see, e.g., the review by Schultz and Lynn [1]) lies between these two curves. The open squares are transformations by (6) and (7) (assuming the validity of the fitted $m = 1.9$ Makhovian) of the median depths generated by *the simulations of Valkealahti and Nieminen [5]. The* inverted triangles are the Monte Carlo results of Jensen and Walker [11], and the diamonds those of Ghosh *et al* [6].

fitted their (non-Makhovian) Al and Cu data to the empirical power law

$$z_{1/2} = (332(80)/\rho)E^{1.6(1)} \text{ Å} \tag{4}$$

where ρ is the material density in g cm^{-3}. Although the measurements were made for incident energies E below 6 keV, it has been common practice to use equation (4) to energies as high as 50 keV; there has been no evidence to support such an extensive extrapolation. The power law relationship

$$z_0 = (A/\rho)E^n \text{ Å} \tag{5}$$

is generally used with $A = 450$ and $n = 1.6$ to deduce values for substitution into equation (3), although its exact origin is unclear. It is interesting to consider the consequences of the seemingly small variations in A and n found in the literature on subsurface defect profiling applications. Figure 3 presents a summary of median penetration depths for Al ($\rho_{Al} = 2.7$ g cm^{-3}) measured or simulated by other researchers. Expressions linking z_0, $z_{1/2}$ and $\bar{z}$ are relatively simple to derive for a Makhovian distribution, viz.

$$\bar{z} = \Gamma(1 + 1/m)z_0 \tag{6}$$

where Γ is a gamma function and

$$z_{1/2} = (\ln 2)^{1/m} z_0. \tag{7}$$

The simple scaling between $z_{1/2}$ and ρ found in equations (4) and (5) has often been assumed to be valid for elements of any ρ. Since the evidence supporting this is based on measurements on Al, Cu and Si this generalization is somewhat optimistic—a conclusion supported by recent experimental work on Pd overlayers on Al [7].

We have made a detailed experimental study of positron stopping in Al and Au for incident energies in the range 0–50 keV [8–10]. The results of this work suggest that the simple dependence of $z_{1/2}$ on ρ—equation (4)—is invalid. The experiments are supported by new Monte Carlo simulations [11], which are also in good agreement with recent positron backscattering measurements [12–14]. In the following section the binary sample technique used in the new measurements is described in detail.

2. The binary sample technique

In this study we follow in essence the approach of Mills and Wilson of measuring the transmission coefficient of positrons through a known thickness of material. There are, however, two important differences. Firstly, in this study the annihilation lineshape or S-parameter method (see below) is used to measure the transmission coefficients, an approach also used in defect profiling applications. Secondly, the use of the S-parameter method allows the transmitted positrons to remain in a solid medium, providing a method for reducing uncertainties rooted in backscattering effects; it has been suggested in the past [1] that the non-Makhovian form of Mills and Wilson's results for $P(E, z)$ was due to incorrect accounting for backscattering in the experiment. This seems unlikely since Mills and Wilson used an elaborate experimental set-up which should have correctly accounted for backscattering effects to first order.

In slow-positron implantation spectroscopy a series of measurements of the mean Doppler broadening of the annihilation gamma-ray line at 511 keV is made for a set of discrete incident positron energies E. The Doppler broadening of the annihilation line is described by the standard shape parameters S or W, which are characteristic of the site at which the annihilation occurs; in this way the location of the annihilating positron is 'tagged'. (Both S and W are related to the linewidth: S is the ratio of the central area of the annihilation photopeak to its total area, and W is the ratio of the sum of the two areas of the wings of the peak to its total area.) In principle any characteristic parameter (for example mean positron lifetime) would serve to tag the annihilation site; measurement of the S- or W-parameter by detection of the annihilation gamma-rays by a high resolution Ge detector is by far the most straightforward and efficient. In the current studies we are interested only in determining whether positrons are annihilated in an overlayer or the substrate; surface effects, such as the emission of work function positrons or of free positronium, are reduced by ensuring that the surface is atomically dirty and that the positron diffusion length in the subsurface region is very short. However, at incident positron energies of a few keV a fraction of positrons will always be able to return to the surface (often prior to thermalization) and their annihilation there, or as positronium in the vacuum above, will contribute to—and change—the measured lineshape parameters. This will be evident in the experimental results presented later; suffice it to say here that data below a few keV are generally disregarded when fitting to a simple two-state model is carried out. In addition,

positronium formation was monitored independently by continuously measuring the ratio of gamma-ray counts in the 511 keV photopeak to the total counts in the spectrum (see [1]), and was found to be significant only below $E = 1$ keV. As a result it is difficult to draw reliable conclusions from studies at low E values (and/or on very thin overlayers).

In all the experimental work described below monoenergetic positrons with E between 1 and 50 keV were implanted into layered samples mounted in the magnetic transport positron beam apparatus described in detail by Hutchins *et al* [15]. The sample targets were epilayers of one material (A) on a substrate of a different material (B). At some incident positron energy E the mean lineshape parameter (S or W; we shall use S here) is, at energies above those for which surface effects are apparent, a linear combination of contributions from A and B;

$$S(E) = F_A(E)S_A + [1 - F_A(E)]S_B \tag{8}$$

where $F_A(E)$ is the fraction of positrons annihilated in the overlayer. If S_A and S_B are known (and, as shown later, these can be usually measured independently) then the mean $S(E)$ directly yields $F_A(E)$. One can then proceed experimentally in two ways: (a) measure $F_A(E)$ for a sample with known epilayer thickness and determine E for which $F_A = \frac{1}{2}$ (the thickness of A is then the median implantation depth for positrons of energy E), or (b) measured F_A at a constant E as a function of the thickness of the epilayer A (the derivative of $1 - F_A$ with respect to layer thickness then yields the implantation profile).

It is important to ensure that positrons backscattered from the sample target are effectively lost from the system; if returned to the sample at lower energies the measured implantation profile would be distorted. This is prevented by passing the incident positrons through an $\boldsymbol{E} \times \boldsymbol{B}$ field set to deflect the beam laterally by one diameter (as viewed on a phosphor screen mounted behind a channel plate detector, with the sample raised); backscattered positrons are deflected once more and cannot then pass through a circular aperture to the electrostatic field, which would reflect them back to the target. If any positrons backscatter from the aperture, they experience a third $\boldsymbol{E} \times \boldsymbol{B}$ deflection by one diameter and hence miss the target on their return.

An ideal sample would clearly consist of a single material that gives rise to one characteristic S-parameter at depths less than some known value and a second S-parameter at depths greater than that value. This ideal is approximated well by a binary (AB) sample if the following conditions are met:

(a) A and B have measurably different S-parameters;
(b) they have similar mass density;
(c) they have similar backscattering coefficients; and
(d) they have very small positron diffusion lengths (so that a negligible fraction of thermalized positrons are able to diffuse across the interface between A and B).

Further, there should be negligible corruption of data due to trapping and annihilation at interfaces.

The samples used in the measurements were (i) a wedge shaped Al film deposited on a glass microscope slide, (ii) seven glass microscope slides covered with between one and ten Al foils of thickness 7000(±190) Å or 7770(±200) Å and (iii) seven 0.5 mm thick, 25 mm square W sheets covered with between one and ten Au foils of thickness either 1038(±15) Å or 1181(±15) Å. The extent to which these samples satisfy criteria (a)–(d) above will be discussed below.

3. Sample preparation

3.1. Aluminium wedge

The Al wedge overlayer was deposited on an (optically flat) glass microscope slide. The slide was held horizontally 20 cm above a BN crucible containing pieces of 99.99% purity Al wire, above which was fixed an Mo foil collimator. These elements were housed in a cylindrical glass vessel pumped to a base pressure below 10^{-4} Pa by a liquid-N_2-trapped diffusion pump system. The approximately linear increase in overlayer thickness was achieved by passing a stainless steel shutter at a constant rate over the glass substrate during deposition. In order to maintain cleanliness the driver motor was mounted on the outside of the solid stainless steel top plate; a strong (SmCo) magnet was pulled across the plate by a rotating screw thread mechanism, acting in turn on a similar magnet attached to the shutter on the underside (i.e., the vacuum side) of the plate. The BN crucible, chosen to minimize O contamination [16], was resistively heated to evaporate the Al which was deposited at a rate of about 40 Å s^{-1}. This procedure has earlier been found to produce homogeneous growth of 1000 Å thick films [17]. Many samples were made under various experimental conditions and stored under vacuum. Each was studied by electron microscopy and the sample exhibiting the most uniform appearance was chosen for the positron measurements.

The thickness profile of the overlayer was measured by Michelson interferometry as follows. Al was also deposited on a second (dummy) glass slide, held alongside the intended sample. A channel, approximately 1 mm wide, was made along the entire length of the Al layer on the edge of the dummy slide adjacent to the sample slide. (The Al was removed by gentle, continuous scraping to reveal the glass substrate; repeatability checks confirmed that this procedure involved negligible disturbance of the glass substrates.) Fringe shifts of monochromatic light reflected from the top surface of the Al and the glass substrate channel were measured along the wedge, and the overlayer thickness thereby determined to within ±100 Å. The validity of this procedure was checked thoroughly by (a) confirming that the profile was not measurably dependent on lateral position across the slide, and (b) measuring similar profiles on dummy and sample slides. The profile for the sample used is shown in figure 4.

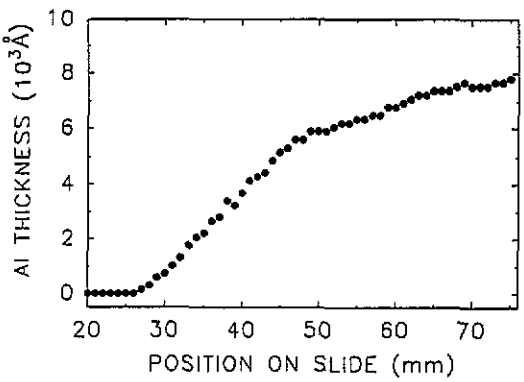

Figure 4. Evaporated Al wedge thickness, measured by Michelson interferometry, against microscope slide position.

The quality of the Al wedge samples was assessed by electron microscopy; micrographs were taken both at the glass–Al boundary and at several positions across the overlayer. The samples were transferred or stored under Ar gas.

3.2. Aluminium foils

In order to study the implantation of positrons of energies up to 50 keV thicker overlayers were required. A set of seven Al on glass samples with progressively thicker Al overlayers were produced by laying down either one, two, three, four, six, eight or ten Al foils on microscope slides. The thicknesses of the foils, individually measured by weighing pieces of known area and assuming bulk density, were (from two batches) 7000 ± 190 Å or 7770 ± 200 Å. The foils were mounted whenever possible in dry conditions by pressing the slide gently on to them, laid singly on lint-free tissue. To aid adhesion a fine spray of acetone was occasionally used. On one microscope slide up to three square samples of different thicknesses could be built up.

3.3. Goil foils

A set of seven 25 mm square, 0.5 mm thick polycrystalline W foils were used as substrates to support two, three, four, six, seven eight or ten Au foils. The thicknesses of the (nominally 1000 Å) foils were determined, again by weighing, to be 1036 ± 15 Å. Dry adhesion of the foils to each other and to the substrate was in this instance achieved in every case.

The samples, of all three types described above, were mounted in the positron beam apparatus on a simple post, with xyz positioning capability, and installed into the vacuum system immediately after being laid down. No cleaning of the sample–vacuum interface, or sample annealing, was carried out so that work function positron and positronium emission were minimized and their effect on the measured parameters kept to a negligible level. The effect of epithermal positron and associated positronium emission can, however, be seen in the experimental data at low incident positron energies, and this is discussed later.

4. Suitability of samples

With the aim in mind of measuring $P(E, z)$ and/or $z_{1/2}$ in Al and Au, the extent to which the binary systems chosen (i.e. Al-glass, Au–W) satisfy criteria (a)–(d) listed in section 3 above should be considered carefully—as should, in the case of multifoil samples, the influence of annihilation at foil–foil interfaces.

The data shown in figures 5 and 6 illustrate that criterion (a)—the need for measurably different S- (or W-) parameters in the two elements of the binary system—is matched by the Al–glass samples; Au–W also satisfies the criterion if S is used (not W—see later)—but with a smaller percentage difference than for Al–glass.

Criteria (b) and (c) are linked in that as far as possible the binary system should be as homogeneous (to the incident positrons) as possible; ideally, overlayer and substrate would be in all respects identical apart from their S-parameters. The density of the glass microscope slide was measured to be 2.53 ± 0.05 g cm^{-3}, and that of the evaporated Al has been measured by others (using the same deposition technique) to be 2.65 g cm^{-3}, only about 2% lower than that for the bulk metal (or the foils) and within 5% of the density of the glass slide. For Au foils and W substrates the measured densities were found to agree well with the accepted bulk value for both of 19.3 g cm^{-3}. The positron backscattering coefficient η_+ for glass was estimated by comparing, for the same implantation energy, the

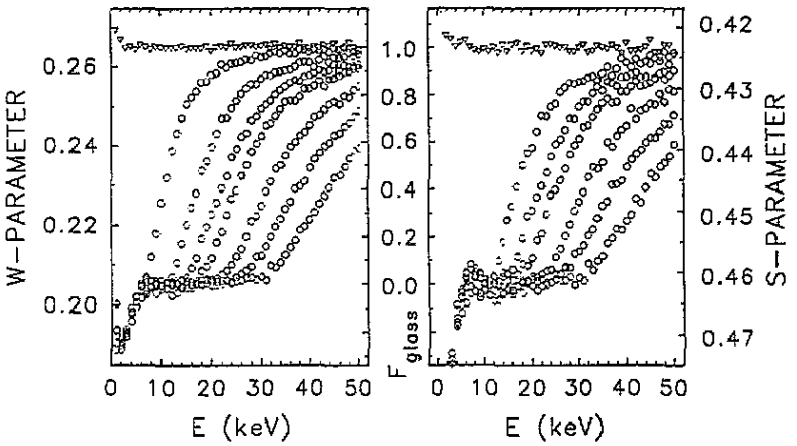

Figure 5. Measured W-parameter (left) and S-parameter (right) against incident positron energy for glass (▽) and (from left to right) one, two, three, four, six, eight and ten 7000(190) Å thick Al foils mounted on a glass substrate (○). The central scale shows the fraction (F_{glass}) of the incident positrons annihilating in the glass.

annihilation count rate in uncoated glass with that in a thick Al sample. This count rate is proportional to $1 - \eta_+$. For example, for $E = 7$ keV, assuming $\eta_+(\mathrm{Al}) = 12\%$ [12] then $\eta_+(\mathrm{glass}) = 11\%$. The results of [12] also imply that $\eta_+(\mathrm{Au}) \simeq \eta_+(\mathrm{W})$ over a range of implantation energies.

The positron diffusion lengths L in all four materials used were independently determined by measuring $S(E)$ for thick samples of each. L values are deduced by first translating directly the $S(E)$ results, such as those presented in figure 5 for uncoated glass and (below 30 keV) for thick Al overlayers, into $F_S(E)$—i.e. the fraction of positrons diffusing to the surface as a function of implantation energy. L is then obtained by fitting $F_S(E)$ using equation (1); if a Gaussian derivative form for $P(E, z)$ is used (i.e. equation (3) with m= 2) then

$$F_S(E) = 1 - 2A \exp(A^2) \int_A^\infty \exp(-y^2)\,\mathrm{d}y \tag{9}$$

where $A = z_0/2L$; L is the only fitting parameter.

In figure 5 it is the deviation of $S(E)$ at low E values that represents diffusion to the surface, and the first-order fitting procedure described above gave the values for L listed in table 1.

Table 1. Diffusion lengths L deduced from fits to $S(E)$ data.

Sample component	L (Å)
Al (deposited)	300 ± 50
Al (foils)	800 ± 100
Glass slide	300 ± 50
Au (foils)	120 ± 20
W (foil)	120 ± 20

The integrity of measured implantation profiles is undermined by diffusion effects only if the overlayer thickness is small (i.e. of the same order as the diffusion length), so that the determination of its characteristic S- or W-parameter is made impossible, by diffusion either to the surface, to the interface, or into the substrate species. This was the case, for example, for a single Au foil—and for two Au foils the additional uncertainty arising from diffusion effects was allowed for by larger error bars on the measured parameters. When $z_{1/2}$ values (total overlayer thicknesses) are much greater than L then the fraction of positrons that diffuse out of the overlayer becomes negligible.

A second consequence of diffusion that has to be considered is the movement of positrons to, and subsequent annihilation at, interface regions between overlayer foils or between species. In a multifoil overlayer, with N foils of thickness d, let there be an effective distance Δd, on either side of each interface, from which positrons can diffuse to the interface. Then the fraction of positrons initially implanted into the overlayer system that diffuse to the interfaces (neglecting the extreme two) is to first order $2N\Delta d/Nd = 2\Delta d/d$, which is independent of N. The measured S parameter is then characteristic of the foils plus interfaces system; for example, one measures $(2\Delta d/d)S_{\text{interface}} = (1 - 2\Delta d/d)S_{\text{foil}}$ instead of S_{foil}. Nevertheless, this parameter is still a valid measure of the total fraction of implanted positrons stopping between its boundaries. This assertion is supported by the identical values of measured overlayer lineshape parameters shown in figure 5 for different numbers of foils. Diffusion to the interface in the Al wedge–glass system is discussed in section 4.

As intimated earlier, raw $S(E)$ or $W(E)$ data are corrupted by the effects of epithermal positron emission only at incident energies below 1 keV. It is assumed throughout that any positrons diffusing to the exit surface are trapped and annihilated there (figure 5 demonstrates this diffusion at E below 6 keV). However, at low enough incident energies a fraction of the positrons return to the surface prior to thermalization and pass through the surface region into the vacuum [18, 19]; escaping positrons that pick up an electron and form singlet (para-)positronium [20] decay within sight of the detector, thereby changing the measured mean lineshape parameter. This effect is seen in figure 5, where it is shown to be unimportant at incident energies above 1 keV.

5. Experimental results

Raw data for S- and W-parameters versus implantation energy for Al foils on glass samples are shown in figure 5; both are directly converted to the fraction of positrons penetrating the foils and being annihilated in the glass ($1 - F_A(E)$, equation (8)) by assuming directly measured values for S (or W) in the foils and in the glass. It is clearly seen from figure 5 that the fractional increase in W between Al and glass (almost 30%) is much larger than the change in S (about 9%), and the W data are consequently smoother and thus to be preferred. For Au on W samples however, the converse is true; W-parameters for the two metals were found to be very similar, and $S(E)$ had to be used. It is clear that there is no hard and fast rule governing the choice of S- or W-parameter; historically researchers engaged in defect studies using the Doppler broadening technique have chosen to use either S- or W-parameters, without considering fully which parameter might be better suited to describing a given system. This was in the past largely due to the magnitude of sophistication such a task would require with traditional data collection techniques. One should ideally maximize the difference in lineshape parameter between bulk and defect states. The parameter used may not even involve the standard approach of taking the ratio of areas within the photopeak,

but may involve some other mathematical manipulation of the spectrum. Computerized data collection systems have made its straightforward to export photopeak spectra to a PC data file, making the task of optimization a relatively simple programming task.

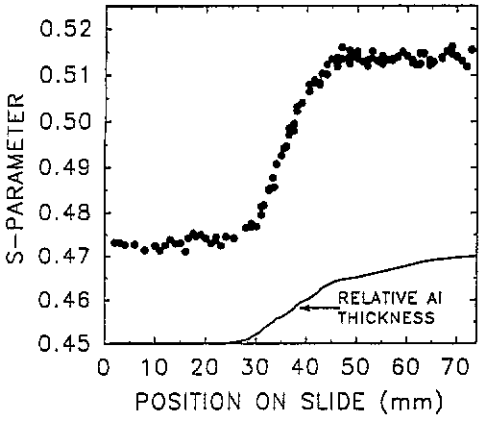

Figure 6. Measured S-parameter against microscope slide position for 7 keV positrons incident on the Al wedge sample.

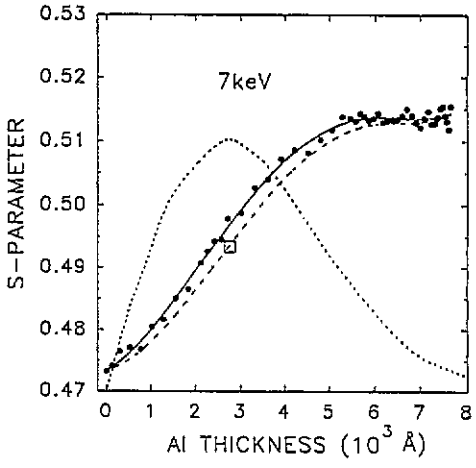

Figure 7. Measured S-parameter (circles) against overlayer thickness for 7 keV incident positrons. The full curve is a spline fit through the data points (see [8]) and the square the median penetration depth predicted by Mills and Wilson's empirical law (equation (4)). The broken curve is a corrected fit, discussed in the text, which allows for diffusion to the interface; the relative fractions of positrons diffusing to the interface are represented by the dotted curve.

Figures 6 and 7 illustrate how $P(E, z)$ is determined using the wedge sample. Figure 6 shows the mean S-parameter for a 3 mm diameter, 7 keV positron beam implanted in the wedge sample, which is moved across the beam in 0.5 or 1 mm steps. A first-order calculation invoking diffusion lengths from table 1 allows one to estimate that approximately 13% of 7 keV positrons implanted into a system with an overlayer of thickness equal to the appropriate $z_{1/2}$ are able to diffuse to the interface and be annihilated there. It is impossible to correct for the effects of diffusion without knowing the S-parameter associated with the interface; however, in an attempt to do so we note that the $P(E, z)$ derived by direct differentiation of the raw data of figure 6 is similar in shape to the Monte Carlo simulation of Jensen and Walker [11] but shifted to slightly lower depths z (refer forward to figure 8), and that in addition the median implantation depth suggested by the raw data is 2380 Å, in comparison to the 2818 Å calculated using equation (4) (figure 7). Figure 7 illustrates how both the discrepancies are overcome by correcting for diffusion to an interface state that has a higher S-parameter than the Al overlayer. First, Padé or cubic spline fits are made to the raw data (the former being the ratio of two quadratics); the fitted S-parameter at 2818 Å is reduced to the average of S_{Al} and S_{glass} by assuming that a fraction F_I (13%) of the positrons are annihilated from the interface state with $S_I = 0.649$. Using this, F_I is then reduced progressively as the Al thickness decreases or increases from 2818 Å, and the appropriate correction $F_I S_I$ made to S. The results is the broken curve in figure 7, which is differentiated to yield the $P(E, z)$ shown. The profile so produced agrees very well with the simulation shown in figure 8.

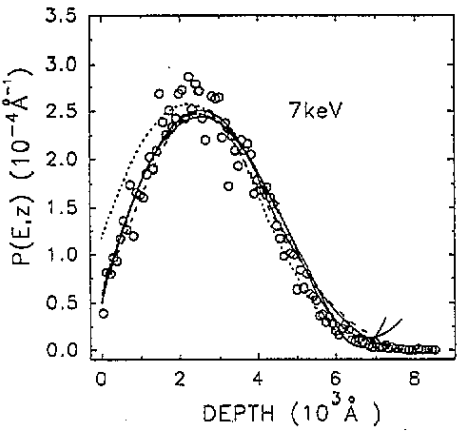

Figure 8. Implantation profiles $P(E, z)$ for 7 keV positrons in Al: the full curves are generated by differentiating cubic spline fits to the corrected experimental data in figure 7 with one, two and three knots. The broken curve is produced by adopting a similar procedure to a Padé fit; the dotted curve is the differential of the uncorrected data (i.e. the full curve in figure 7). The circles are the Monte Carlo results of Jensen and Walker [11].

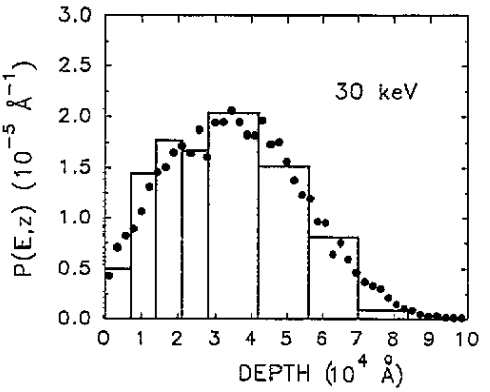

Figure 9. Experimentally derived implantation histogram $P(E, z)$ for 30 keV positrons in Al derived from the data in figure 5. The circles are the Monte Carlo results of Jensen and Walker [11].

Implantation profiles deduced from discrete foil overlayers are of necessity histograms rather than continuous distributions. The example shown in figure 9, along with the Monte Carlo simulations of Jensen and Walker [11], takes the differences between the numbers of 30 keV positrons stopping in 1, 2, 3, 4, 6, 8, 10 and 12 Al foils.

The major results of the experiments described above underline the dependence of implantation parameters on the target material.

(a) The shape of $P(E, z)$ for Al (and therefore, the authors believe, Si) is best defined by [8]

$$P(E, z) = -(\partial/\partial_z)\exp\{-[(z/z_\alpha(E))(1 + z/z_\alpha(E))^2]^{1.28}\} \tag{10}$$

where $z_\alpha = 2.58 z_{1/2}$, $z_{1/2}(E) = 129E^{n(E)}$, and $n(E) = 1.45 + 0.053 \ln E$.

$P(E, z)$ for Au was found to be best described [10] by the Makhovian

$$P(E, z) = -(\partial/\partial_z)\exp\{-[z/z_0(E)]^{1.7}\}. \tag{11}$$

(b) The form of equation (5) can be used for $z_{1/2}(E)$ for Al and Au, but neither is adequately described by the long-accepted parameters A and n. For Al, $A = 2.62 \pm 0.38$ μg cm^{-2} keV^{-n} and $n = 1.71 \pm 0.04$, and for Au $A = 8.31 \pm 2.78$ μg cm^{-2} keV^{-n} and $n = 1.42 \pm 0.08$ [10]. (These A values correspond to 262 and 831 in equation (5).)

(c) All the experimental results are in excellent agreement with the Monte Carlo simulations of Jensen and Walker [11].

6. Conclusions

The binary sample method for the measurement of implantation profiles and median depths for positrons in solids has been shown to be effective for energies above a few keV. The

measured implantation profile rises more sharply at low z than the Gaussian derivative in common use, and this may have implications for the interpretation of depth profiling of near-surface defects by positron implantation spectroscopy. There are other sources of problems in near-surface studies—notably the effect of epithermal positron motion, and possible corruption of data by the return (by a reflecting electrostatic field) of low-energy positrons backscattered from the sample.

The experiments described here could be repeated for any other solid samples, providing that the criteria outlined in section 3 are met as closely as possible.

Acknowledgments

The authors are grateful to the SERC for financial support, and to the School of Environmental Sciences at the University of East Anglia for use of their electron microscopy facilities in characterizing samples. We should also like to thank Vinita Ghosh of Brookhaven National Laboratory for communicating the Monte Carlo results shown in figures 2 and 3.

References

[1] Schultz P J and Lynn K G 1988 *Rev. Mod. Phys.* **60** 701
[2] Vehanen A, Saarinen K, Hautojärvi P and Huomo H 1987 *Phys. Rev.* B **35** 4606
[3] Nielsen B, Lynn K G, Vehanen A and Schultz P J 1985 *Phys. Rev.* B **32** 2296
[4] Mills A P Jr and Wilson R 1982 *Phys. Rev.* A **26** 490
[5] Valkealahti S and Nieminen R M 1984 *Appl. Phys.* A **35** 51
[6] Ghosh V J, Welch D O and Lynn K G 1993 *Proc. 5th Int. Workshop on Slow Positron Beams* ed E Ottewitte and A Weiss (New York: AIP) at press
See also McKeown M, Lynn K G and Welch D O, referred to in
Asoka-Kumar P and Lynn K G 1990 *Appl. Phys. Lett.* **57** 1634
Ritley K A, McKeown M and Lynn K G 1990 *Positron Beams for Solids and Surfaces* ed P J Schultz, G R Massoumi and P J Simpson (New York: AIP) p 3
[7] Nielsen B, Lynn K G, Leung T C, Van der Kolk G J and Van Ijzendoorm 1990 *Appl. Phys. Lett.* **56** 728
[8] Baker J A, Chilton N B, Jensen K O, Walker A B and Coleman P G 1991 *J. Phys.: Condens. Matter* **3** 4109
[9] Baker J A, Chilton N B and Coleman P G 1991 *Appl. Phys. Lett.* **59** 164
[10] Baker J A, Chilton N B, Jensen K O, Walker A B and Coleman P G 1991 *Appl. Phys. Lett.* **59** 2962
[11] Jensen K O and Walker A B submitted
[12] Coleman P G, Albrecht L, Walker A B and Jensen K O 1992 *J. Phys.: Condens. Matter* **4** 10311
[13] Mäkinen J, Palko S, Martikainen J and Hautojärvi P 1992 *J. Phys.: Condens. Matter* **4** 503
[14] Massoumi G R, Hozhabri N, Jensen K O, Lennard W N, Lorenzo M S, Schultz P J and Walker A B 1992 *Phys. Rev. Lett.* **68** 3873
[15] Hutchins S M, Coleman P G and West R N 1985 *Positron Annihilation* ed P Jain, R M Singru and K P Gopinathan (Singapore: World Scientific) p 983
[16] Glang R 1990 *Handbook of Thin Film Technology* ed L I Maissel and R Glang (New York: McGraw-Hill) p 1
[17] Saunders J V 1971 *Chemisorption and Reactions on Metal Films* ed J R Anderson (New York: Academic) p 1
[18] Nielsen B, Lynn K G and Chen Yen-C 1986 *Phys. Rev. Lett.* **57** 1789
[19] Coleman P G, Goodyear A and Knights A P 1993 *Proc. 5th Int. Workshop on Slow Positron Beams* ed E Ottewitte and A Weiss (New York: AIP) at press
[20] Howell R H, Rosenberg I J and Fluss M J 1986 *Phys. Rev.* B **34** 3069